

Article

Effects of n-Al₂O₃ and μ-TiCN on Microstructure and Mechanical Properties of Al₂O₃ Composite Ceramics Manufactured by Material Extrusion and Photo-Polymerization Combined Process

Xin He ¹, Jie Xu ^{2,*} and Weixi Ji ^{1,*}¹ School of Mechanical Engineering, Jiangnan University, Wuxi 214122, China; 7180832001@stu.jiangnan.edu.cn² Department of Astronautical Science and Technology, Space Engineering University, Beijing 101400, China

* Correspondence: xujiemechanic@163.com (J.X.); weixiji_jiangnan@outlook.com (W.J.)

Abstract: Alumina (Al₂O₃) composite ceramics with different composition ratio and particle-size distribution were fabricated by the material extrusion and photo-polymerization combined process (MEX-PPM) based on additive-manufacturing (AM) technology in our previous work. These particles were nanosized Al₂O₃ (n-Al₂O₃), micron-sized TiCN (μ-TiCN) and Al₂O₃. Effects of n-Al₂O₃ and μ-TiCN on Al₂O₃ composite ceramics were investigated by characterizing the volume density, EDS spectrum, mechanical properties and microstructure of the prepared samples. It was found that n-Al₂O₃ had a significant effect on the hardness of Al₂O₃ composite ceramics, μ-TiCN, with excellent performance in density, flexural strength and fracture toughness. The Al₂O₃ composite ceramics with optimum contents of 10 wt % n-Al₂O₃ and 30 wt % μ-TiCN showed good microstructure and mechanical properties. Their porosity and volume density were at 4.073% and 4.177 g/cm³, respectively. Their hardness, flexural strength and fracture toughness were at 16.592 GPa, 592.875 MPa and 6.308 MPa/mm². The flexural strength of the ceramics was significantly higher than that of Al₂O₃ ceramics prepared by SLA in document (178.84 ± 17.66 MPa), which had great potential in high-pressure strength structure.

Keywords: Al₂O₃; additives; material extrusion; photopolymerization; additive manufacturing



Citation: He, X.; Xu, J.; Ji, W. Effects of n-Al₂O₃ and μ-TiCN on Microstructure and Mechanical Properties of Al₂O₃ Composite Ceramics Manufactured by Material Extrusion and Photo-Polymerization Combined Process. *Crystals* **2022**, *12*, 745. <https://doi.org/10.3390/cryst12050745>

Academic Editors: Ana Pilar Valerga Puerta, Severo Raul Fernandez-Vidal, Zhao Zhang, Umberto Prisco and George Z. Voyiadjis

Received: 23 April 2022

Accepted: 20 May 2022

Published: 23 May 2022

Publisher's Note: MDPI stays neutral with regard to jurisdictional claims in published maps and institutional affiliations.



Copyright: © 2022 by the authors. Licensee MDPI, Basel, Switzerland. This article is an open access article distributed under the terms and conditions of the Creative Commons Attribution (CC BY) license (<https://creativecommons.org/licenses/by/4.0/>).

1. Introduction

Alumina (Al₂O₃) ceramic has been widely used in cutting tools [1,2], aircraft engines, integrated circuits [3] and medical human joints [4,5] due to its excellent mechanical properties, chemical stability and good economy advantages, etc. For ceramic parts with complex, multimaterial structures and high forming accuracy [6,7], the traditional forming technology is difficult to form through homogeneous composite, which has limited the performance of ceramics. In recent years, the rapid development of additive manufacturing technology can obtain ceramic parts with specific requirements through multilayer stacking [8,9], which has the advantages of free design and rapid prototyping [10,11].

At present, the additive-manufacturing-based photo-polymerization (PPM) technology and material extrusion (MEX) technology are the two most commonly used methods in ceramics fabrication due to the advantages of high precision [12,13], complex structures [14] and multimaterial distribution [15] such as stereolithography (SLA) [16], digital light processing (DLP) [17], extrusion freeforming (EFF) [18], on-demand extrusion (CODE) process [19] and direct ink writing (DIW) [20]. However, because of the limited solid content, the ceramics produce pores in degreasing and sintering, which reduce the compactness and mechanical properties [21].

The particle size and additives [22–24] have an impact on the properties of final ceramics, which are mainly focused on ceramics prepared by traditional technology and

PPM technology. Huai et al. [25] studied the effects of nanosized and micron-sized additives (TiO_2) on Al_2O_3 ceramics. The 0.15 wt % TiO_2 is conducive to the sintering properties of Al_2O_3 ceramics under 1300–1500 °C, and nanosized TiO_2 is more conducive to the bulk density, hardness and wear properties at the same sintering temperature. Wu et al. [26] investigated the effects of particle size and the degreasing process on the densification of Al_2O_3 ceramics. The results show that the samples containing both nanosized and micron-sized particles have the highest compactness. The combination of powder with bimodal particle-size distribution and the vacuum-degreasing process can effectively realize the three-dimensional printing of ceramic products. Zhang et al. [27] studied the effects of fine particles and sintering additives on the properties of Al_2O_3 ceramics prepared by SLA by adding fine particles and sintering additives (TiO_2 and MgO) to ceramics. The best ceramics contain 42.5 wt % coarse particles, 7.5 wt % fine particles, 1 wt % MgO and 3 wt % TiO_2 . The results showed that fine particles can improve the activity of Al_2O_3 ceramics and reduce the sintering temperature. Sintering additives TiO_2 and MgO can improve the solid-state sintering properties of Al_2O_3 ceramics. The final properties of ceramics are determined by the appropriate proportion of particle size and additives.

However, multisize particles and additives could behave differently on ceramics fabricated by MEX technology. The fine particles will reduce the fluidity and printability of ceramic raw materials [28] which limits the performance of finished products prepared by material extrusion technology with strict requirements on the rheology of ceramic raw materials. At present, the effect of multisize particles on ceramics fabricated by MEX technology has not been much studied. The effects of the multisize particles and the additives on Al_2O_3 composite ceramics printed by the material extrusion and photopolymerization combined process (MEX-PPM) [29] have not been analyzed clearly.

In this work, nanosized Al_2O_3 (n- Al_2O_3) and microsized TiCN (μ - TiCN) were selected as additives, the Al_2O_3 composite ceramic green body was printed by the MEX-PPM process proposed in the previous work, and a two-step vacuum-air debinding and sintering were carried out [30]. Effects of n- Al_2O_3 and μ - TiCN on the microstructure and mechanical properties of Al_2O_3 composite ceramic by MEX-PPM additive manufacturing were studied.

2. Materials and Methods

The ceramic powders included microsized Al_2O_3 (μ - Al_2O_3) (particle sizes of 1 μm) and n- Al_2O_3 (particle sizes of 200 nm) (Dongfeng Metal Research Center, Qidong, China), μ - TiCN , Ni, Mo and MgO with particle sizes of 1 μm (Tuopu Metal Materials Co., Ltd., Suzhou, China). A prepolymer solution was prepared from 1,6-hexanediol diacrylate (HDDA) (Changxing Chemical Co., Ltd., Chendu, China), oleic acid (OA) and Diphenyl (2,4,6-trimethylbenzoyl)-phosphate oxide (TPO) (BASF GmbH, Ludwigshafen, Germany) for powder mixing.

To prepare the slurry for ceramic-sample fabrication, 0.15 wt % OA with amphoteric groups were used to modify ceramic powder. A total of 1 wt % TPO was added to HDDA to prepare the prepolymer solution, then the modified powders were mixed into the prepolymer solution by ball milling for 4 h, and the mixed slurry was ultrasonically vibrated and vacuumed to obtain printable ceramic slurry. The ceramic green body was printed using the MEX-PPM additive-manufacturing process, and the tubular furnace (GSL-1700X, Hefei Kejing Material Technology Co., Ltd., Hefei, China) was used for degreasing and sintering. The process is shown in Figure 1.

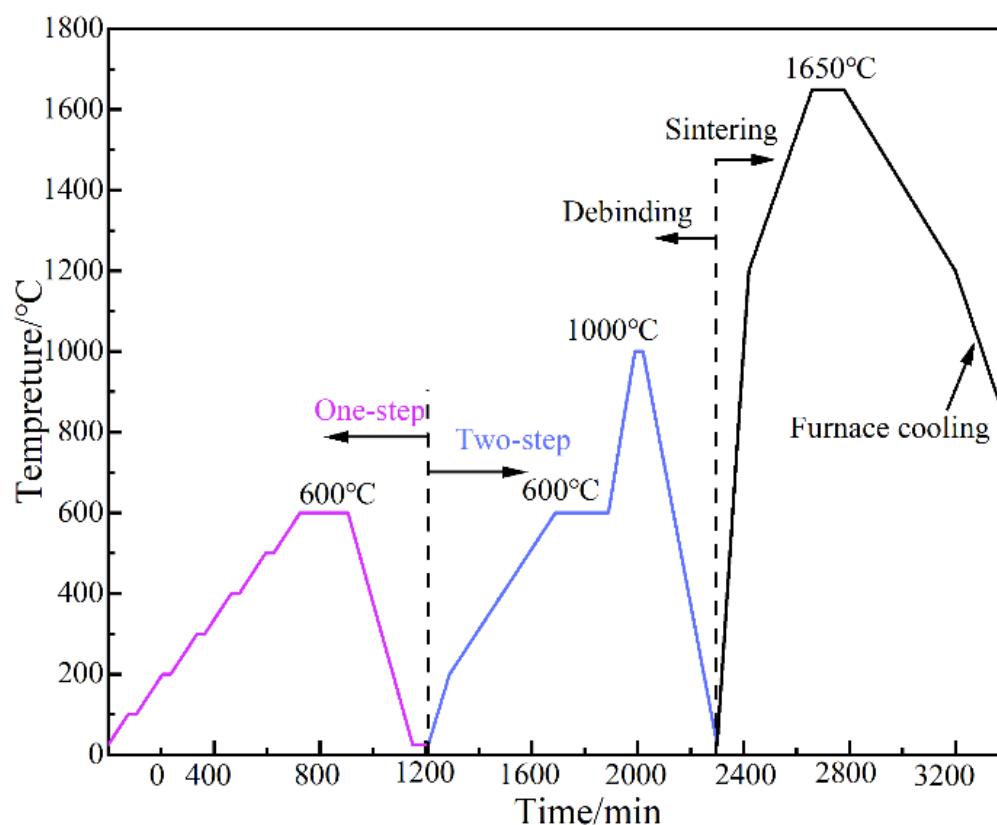


Figure 1. Degreasing and sintering process.

Our previous research results showed that ceramic slurry with viscosity greater than 8.88 Pa·s would limit the printing of MEX-PPM combined process [29]. Thus, 6 kinds of ceramic slurries with the same solid content and maximum viscosity of 8.73 Pa·s were adopted. A nozzle with a diameter of 0.5 mm was used to print ceramic samples at a speed of 5 mm/s. The samples with $n\text{-Al}_2\text{O}_3$ are represented by Sn- x , including Sn1, Sn2 and Sn3, and the samples with $\mu\text{-TiCN}$ are labeled as St- x , including St1, St2 and St3. Through preliminary experiment, the performance of Al_2O_3 composite ceramic sintered body with $\mu\text{-TiCN}$ less than 20 wt % is poor. The minimum content of $\mu\text{-TiCN}$ in the formula sample in this study is 20 wt %. The details of the solid contents of Al_2O_3 composite ceramic slurries are shown in Table 1.

Table 1. The details of solid contents of Al_2O_3 composite ceramic slurries (wt %).

Samples	$\mu\text{-Al}_2\text{O}_3$	$n\text{-Al}_2\text{O}_3$	$\mu\text{-TiCN}$	Ni	Mo	MgO
Sn1	69	5	20	2	2	2
Sn2	64	10	20	2	2	2
Sn3	59	15	20	2	2	2
St1	59	10	25	2	2	2
St2	54	10	30	2	2	2
St3	49	10	35	2	2	2

The microstructure of Al_2O_3 composite ceramics and energy-dispersive spectroscopy (EDS) were characterized using a scanning electron microscope (Evo18, Zeiss, Oberkochen, BW, Germany). The flexural strength was measured using a three-point bending test by electronic universal testing machine (WDW-100KN, Instron Co., Boston, MA, USA); the testing bars were 30 mm \times 4 mm \times 3 mm (length \times width \times thickness) with a span of 20 mm and a loading rate of 0.5 mm/min. Hardness and fracture toughness were measured using a Micro Vickers hardness tester (HV-1000ZCM-XY, Anyi Instrument Co., Ltd., Shanghai, China); 20 indentation points were taken and held pressure at 196 N for 15 s. In addition,

the density was calculated by the Archimedes method. The differences in volume density and mechanical properties of Al_2O_3 composite ceramics under the effect of $n\text{-Al}_2\text{O}_3$ and $\mu\text{-TiCN}$ were calculated by Equation (1).

$$\Delta S_i = S_{ij}(\max - \min) \quad i = n, t; j = 1, 2, 3 \quad (1)$$

where ΔS_i is the difference in volume density and mechanical properties; and S_{ij} is the corresponding Al_2O_3 composite ceramic sample.

3. Results and Discussion

3.1. Effects of $n\text{-Al}_2\text{O}_3$ on the Microstructure and Mechanical Properties

$n\text{-Al}_2\text{O}_3$ with different solid contents was filled into Sn-x type Al_2O_3 composite ceramics; their volume density, mechanical properties and variation-testing results were shown in Figure 2.

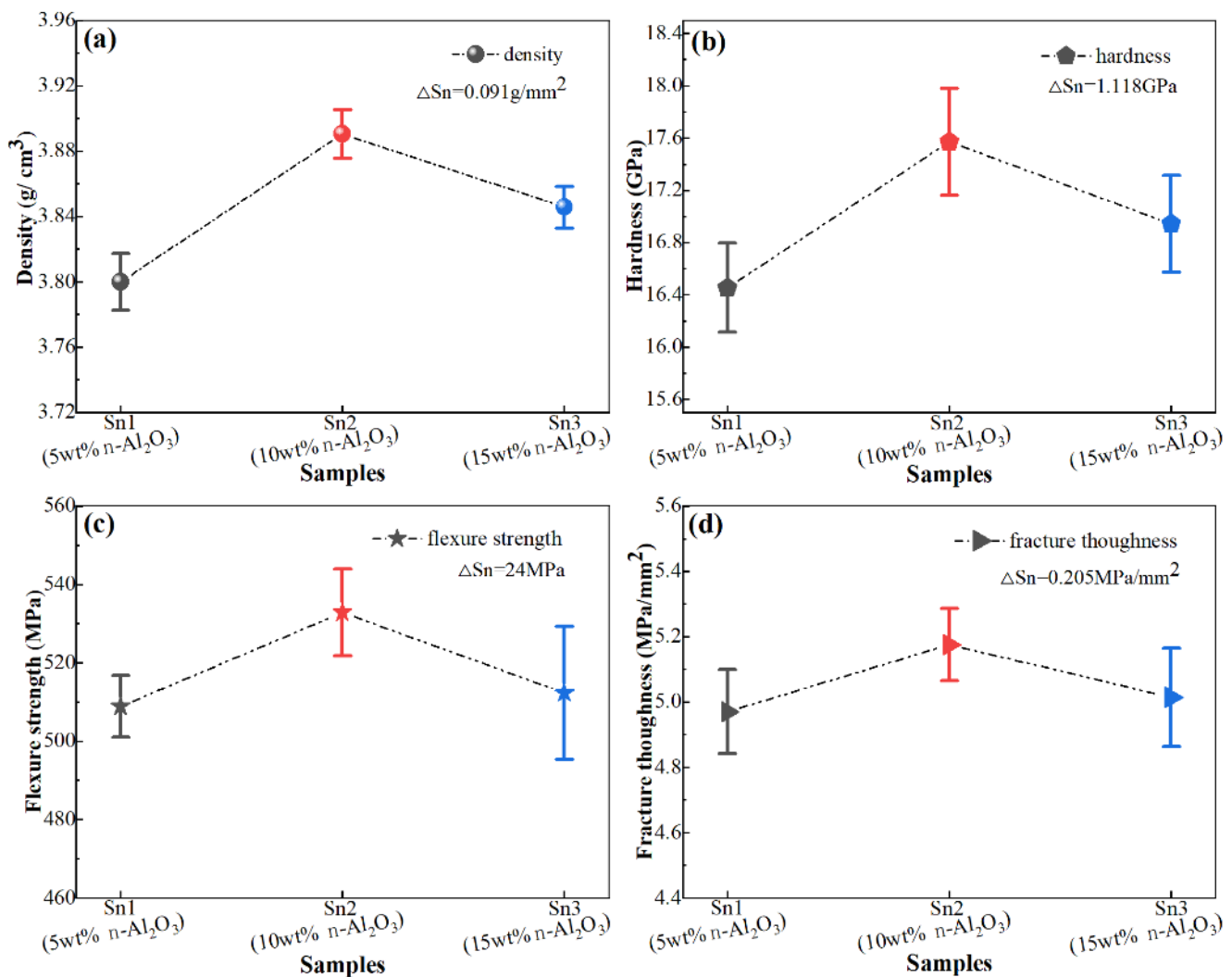


Figure 2. The effects of $n\text{-Al}_2\text{O}_3$ on the properties of Al_2O_3 composite ceramics: (a) density, (b) hardness, (c) flexure strength, (d) fracture toughness.

The solid circle, pentagon, pentagram and triangle in Figure 2 correspond to volume density, hardness, flexural strength and fracture toughness, respectively. The marked colors include gray, red and blue, corresponding to samples Sn1, Sn2 and Sn3, respectively. Among Sn-x type ceramics, Sn2 with 10 wt % $n\text{-Al}_2\text{O}_3$ (red marks in Figure 2) has the best performance. Its volume density is $3.891 \text{ g}/\text{cm}^3$, hardness is 17.5719 GPa , fracture

toughness is 5.5756 MPa/mm² and bending strength is 508.875 MPa. Compared with Sn1 with 5 wt % n-Al₂O₃ (gray marks in Figure 2), the fracture toughness and bending strength of Sn2 are slightly improved, the hardness is significantly improved and the difference in hardness is 1.118 GPa. For Sn3 with 15 wt % n-Al₂O₃ (blue mark in Figure 2), its volume density and mechanical properties were lower than Sn2 and higher than Sn1, which is caused by excessive fine-grained n-Al₂O₃. In addition, the differences in volume density, flexural strength and fracture toughness of Sn-x type ceramics are 0.091 g/cm³, 24 MPa and 0.205 MPa/mm², respectively. According to the above results, n-Al₂O₃ has a significant effect on the hardness of Al₂O₃ composite ceramics. In order to verify that the test results of the above samples are based on the proportioning components designed in Table 1, the EDS spectra of Sn-x type composite ceramics were characterized. Since the mass percentage of other components in the Sn-x type composite ceramics is constant except μ -Al₂O₃ and n-Al₂O₃, the EDS spectrum is the same, as shown in Figure 3.

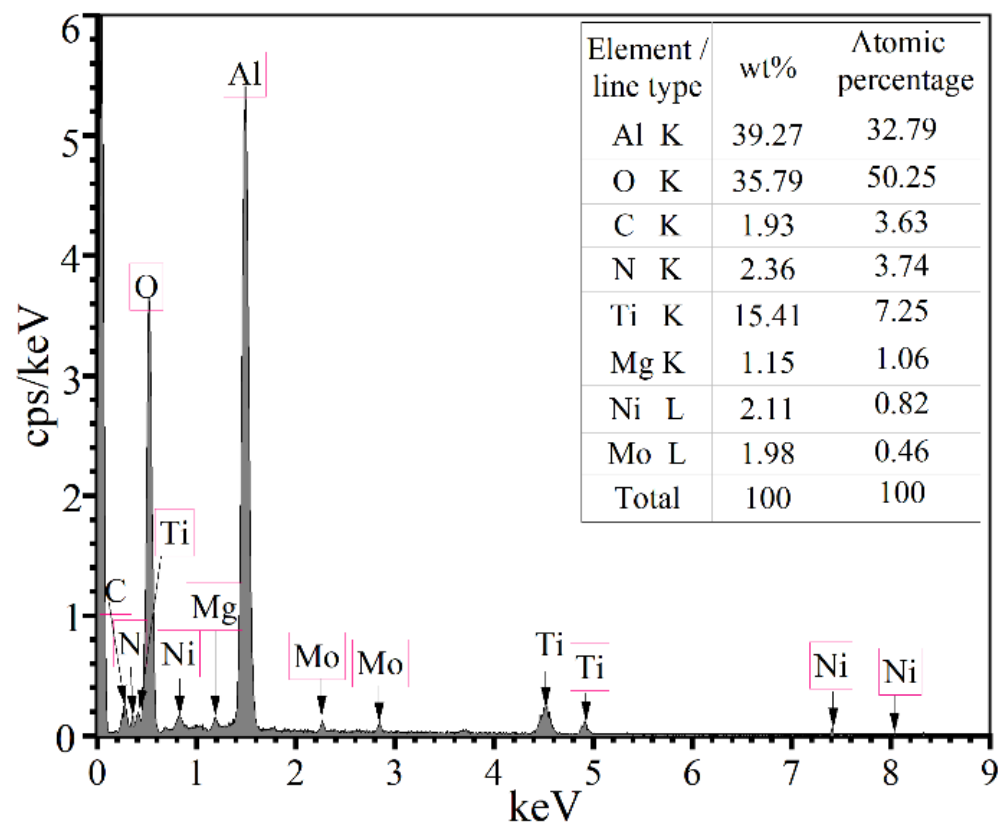


Figure 3. The EDS of Sn-x type Al₂O₃ composite ceramics.

Figure 3 shows the EDS spectrum of random areas on the surface of Sn-x type ceramics. The upward obvious peak signal corresponds to Al, O, C, N, Ti, Mg, Ni and Mo elements, which confirms the existence of Al₂O₃, μ -TiCN, MgO, Ni and Mo components in Sn-x type ceramics. The element content of each component in the EDS spectrum is close to that designed in Table 1, and the error caused by each component element is within 2% of the error range of the EDS spectrum test. The peak corresponding to the Al element is the common content in n-Al₂O₃ and μ -Al₂O₃. To further study the influence of n-Al₂O₃ particles on the properties of Al₂O₃ composite ceramics, the microstructure of Sn-x type composite ceramics was also characterized, as shown in Figure 4.

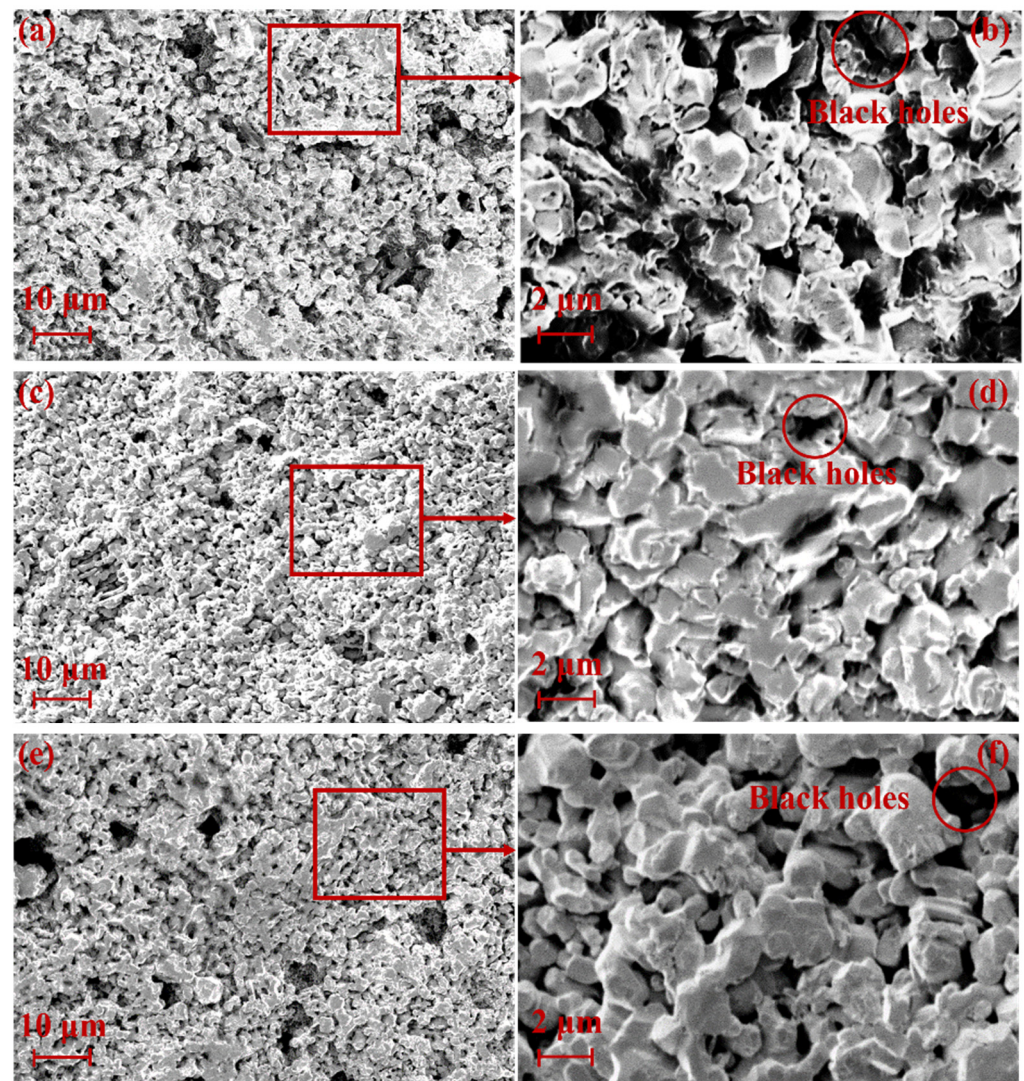


Figure 4. SEM images of the Sn-x type sintered ceramics: (a,b) Sn1, (c,d) Sn2, (e,f) Sn3.

Figure 4 shows the microstructure of Al_2O_3 composite ceramics Sn1, Sn2 and Sn3 at $2000\times$ and $10,000\times$ magnification. Among them, Sn1 (Figure 4a,b) has more pores, with a porosity of 10.664%, followed by Sn3 (Figure 4e,f), with a porosity of 9.589%. Although the number of pores in Sn3 decreases, the macropores are obvious and the pore size is uneven. In comparison, Al_2O_3 composite ceramics Sn2 (Figure 4c,d) are more uniform and dense, with a low porosity of 8.535%. The above phenomenon is that a small amount of n- Al_2O_3 particles per unit volume is not enough to fill the pores between micron particles (black holes in Figure 4b), thus forming a relatively loose composite ceramic structure Sn1 (Figure 4a). On the contrary, excessive n- Al_2O_3 cannot be completely filled into the pores, resulting in agglomeration, forming holes of different sizes randomly distributed in the interior of the ceramic (Figure 4e,f). Only when n- Al_2O_3 particles complement the pores between micron particles to obtain better ceramics. As shown in the SEM of Sn2 with 10 wt % n- Al_2O_3 in Figure 4c,d, the overall structure is more uniform and there are fewer holes, which is consistent with the high density of Sn2 ceramics shown in Figure 2a. In addition, the low hardness, flexural strength and fracture toughness in Figure 2a–c are also caused by inappropriate n- Al_2O_3 particles and a low-pressure compactness structure.

3.2. Effects of $\mu\text{-TiCN}$ on the Microstructure and Mechanical Properties

To study the effects of $\mu\text{-TiCN}$ on Al_2O_3 composite ceramics, it was necessary to characterize the volume density, mechanical properties, EDS spectrum and microstructure

of St-x type ceramics. Figure 5 shows the volume density and mechanical properties of St-x type ceramics with different content μ -TiCN. The optimum content of n- Al_2O_3 in St-x type composite ceramics is 15 wt %.

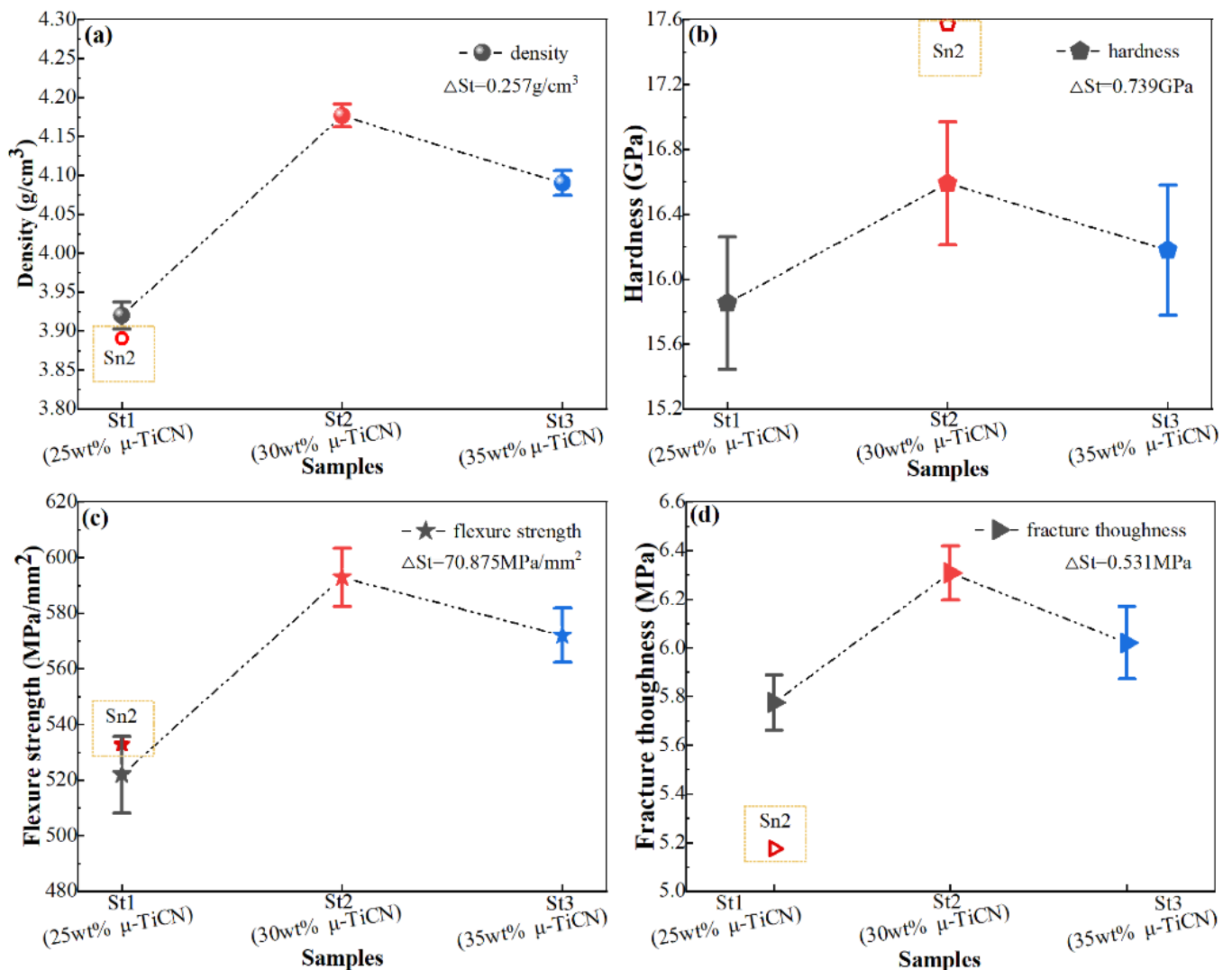


Figure 5. The effects of μ -TiCN on the mechanical properties of St-x type ceramics: (a) density, (b) hardness, (c) flexure strength, (d) fracture toughness.

The solid circle, pentagon, pentagram and triangle in Figure 5 correspond to volume density, hardness, flexural strength and fracture toughness, respectively. The marked colors include gray, red and blue, corresponding to samples St1, St2 and St3, respectively. The meanings of the different symbols in Figure 5 are the same as those in Figure 2. In St-x type composite ceramics, St2 has remarkable properties, with volume density of $4.177\text{ g}/\text{cm}^3$, hardness of 16.192 GPa , flexural strength of 592.875 MPa and fracture toughness of $6.3081\text{ MPa}/\text{mm}^2$ (red marks in Figure 5). Compared with composite ceramic St1, the volume density, flexural strength and fracture toughness of St2 are significantly improved. For composite ceramic St3, its density and mechanical properties are only higher than St1. Nevertheless, the properties of St1 ceramics are still better than Sn2 (red hollow mark in Figure 5). Figure 5 also shows the fluctuation of volume density and mechanical properties of St-x type ceramics under the effects of μ -TiCN, in which the fluctuation of volume density, hardness, flexural strength and fracture toughness are large, with change values of $0.257\text{ g}/\text{cm}^3$, 0.739 GPa , 70.875 MPa and $0.531\text{ MPa}/\text{mm}^2$, respectively, and the differences in density, flexural strength and fracture toughness are greater than that of

Sn-x type ceramics under the effects of n-Al₂O₃ in Figure 2. However, the difference in hardness (0.739 GPa in Figure 5b) in St-x type composite ceramics is less than that in Sn-x type ceramics (1.118 GPa in Figure 2b). This shows that μ -TiCN plays a significant role in improving the volume density, flexural strength and fracture toughness of Al₂O₃ composite ceramics, and n-Al₂O₃ is more beneficial to the hardness. The difference result of the above properties of St-x type ceramics is caused by the change in μ -TiCN content. To verify this conclusion, the EDS spectrum characterization of Al₂O₃ composite ceramics St1, St2 and St3 containing μ -TiCN is carried out, as shown in Figure 6.

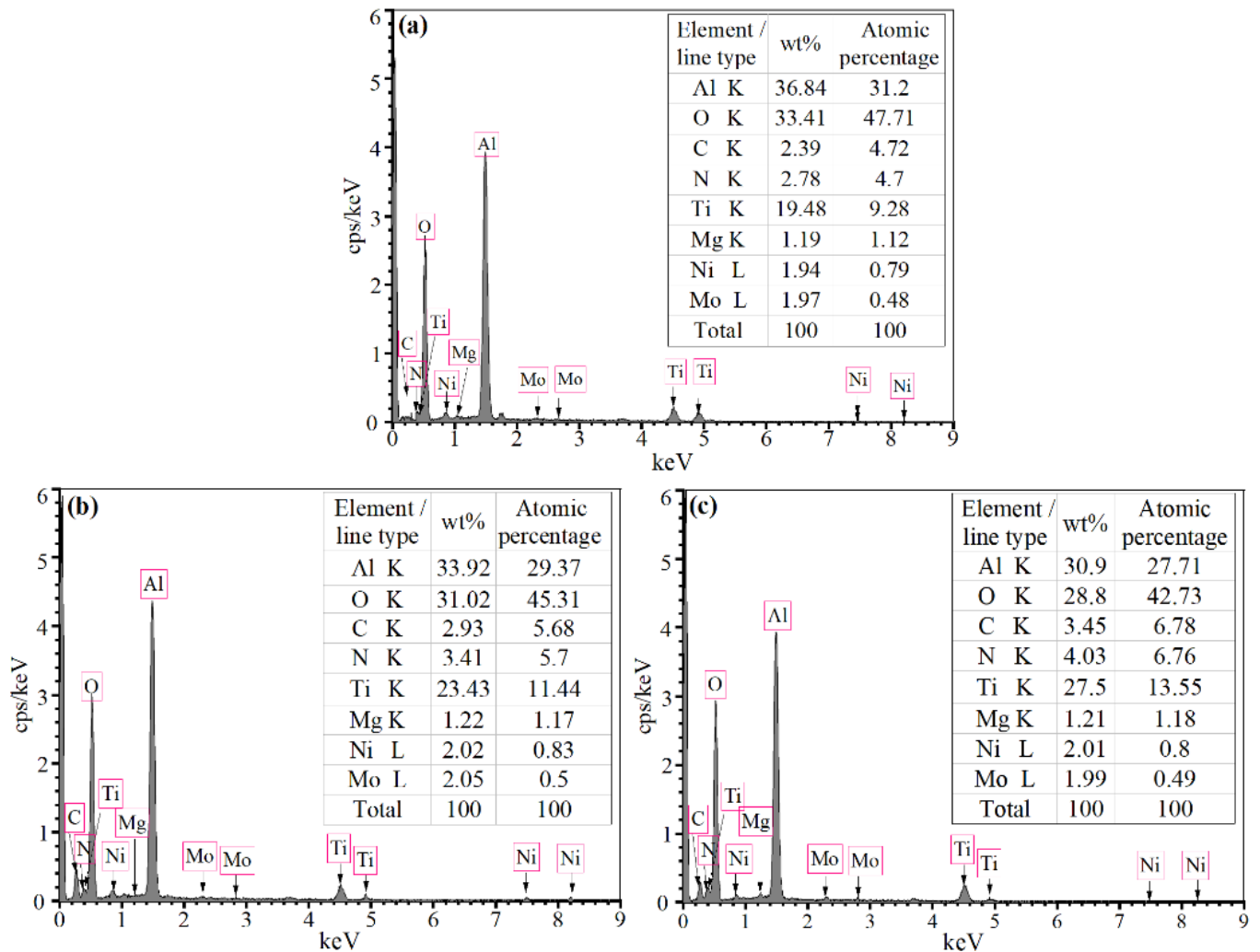


Figure 6. The EDS spectrum of St-x type Al₂O₃ composite ceramics: (a) St1, (b) St2, (c) St3.

Figure 6 shows the obvious peaks corresponding to the Al and O elements, followed by elements Ti, N and C, etc., which indicated the content of Al and O elements in St-x type ceramics is higher. The data table in the EDS spectrum shows that except for Al, O, Ti, N and C elements from Al₂O₃ and μ -TiCN, the content of other elements fluctuates (Mg, Ni and Mo) slightly near the constant value (Figure 6a–c), and the fluctuation value is within 2% of the error range of the EDS spectrum test, which is almost close to the proportion designed in St-x type composite ceramic components.

For Ti, N and C elements from μ -TiCN, the atomic mass and percentage from St1 to St3 measured by the EDS spectrum gradually increase, in which the atomic mass and percentage of Ti elements are (19.658 wt %, 9.421%), (23.589 wt %, 11.519%) and (27.521 wt %, 13.698%), respectively, which is consistent with St1 (19.48 wt %, 9.28%), St2 (23.43 wt %, 11.44%) and St3 (25.7 wt %, 13.55%) designed in Table 1. The above EDS test results verify

that the compactness and mechanical properties of Al_2O_3 composite ceramics are affected by the quality of $\mu\text{-TiCN}$. Therefore, the Al_2O_3 composite ceramic St2 with 30 wt % $\mu\text{-TiCN}$ has good properties.

In addition, the SEM morphology of St-x type ceramics was characterized, and the effects of $\mu\text{-TiCN}$ on microstructure of Al_2O_3 composite ceramics was studied, as shown in Figure 7.

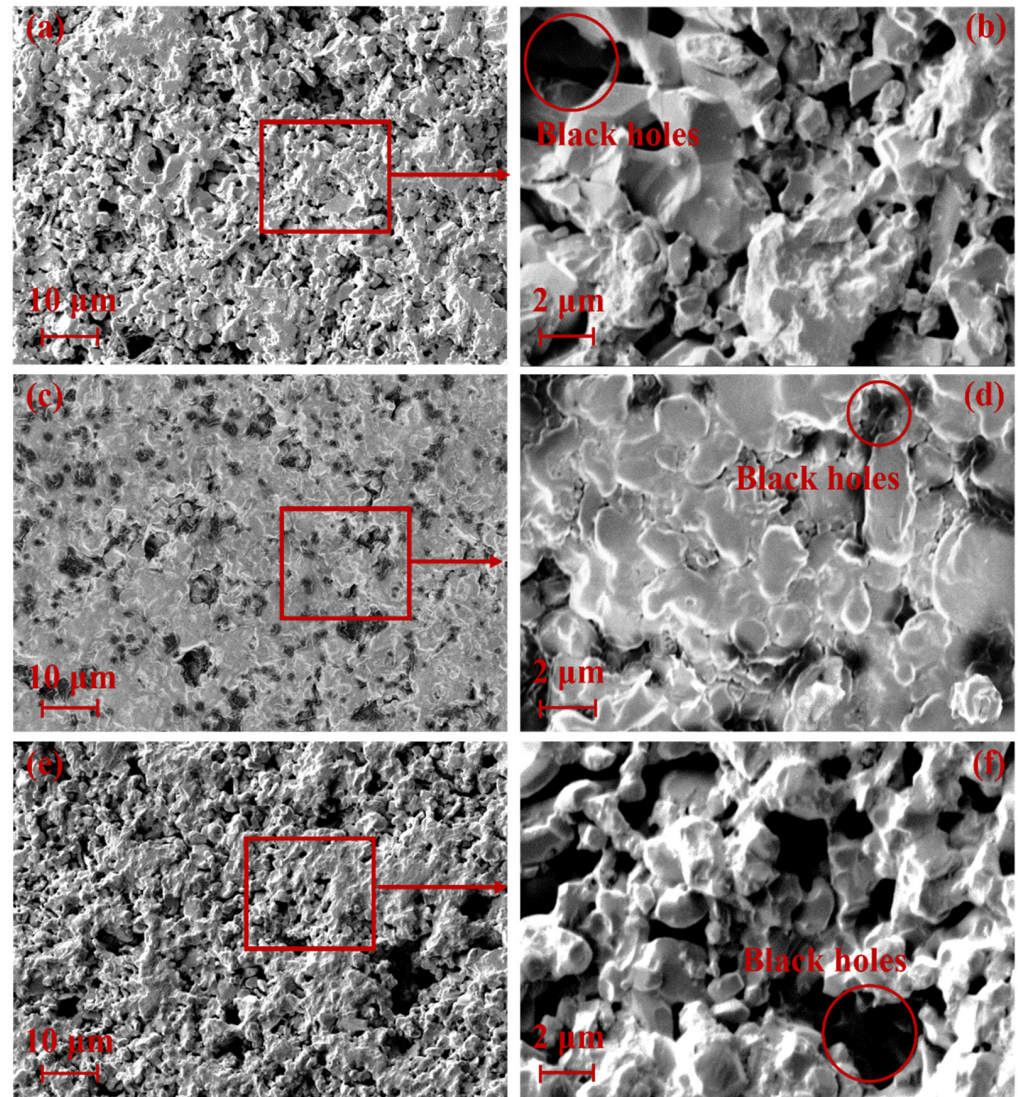


Figure 7. SEM images of the St-x type ceramics: (a,b) St1, (c,d) St2, (e,f) St3.

Figure 7 shows the microstructure of a St-x type Al_2O_3 composite ceramic sintered body under low magnification and high magnification. At low magnification, the compactness of St-x type composite ceramics is better than Sn-x type ceramics.

For St-x type composite ceramics, St1 (Figure 7a,b) has the highest porosity of 8.909%, followed by St3 (Figure 7e,f) with a porosity of 7.184%, and St2 (Figure 7c,d) has a lower porosity of 4.073%. At high magnification, it can also be observed that the significance and randomness of St3 ceramic pores are higher than St1 and St2. In comparison, St2 has a more uniform and dense microstructure (Figure 7c,d), which is consistent with the best volume density of St2 in Figure 5a. In addition, St1 with the lowest volume density (3.92 g/cm^3) in St-x type ceramics is also higher than Sn2 with the best volume density (3.891 g/cm^3) in Sn-x type ceramics.

The above phenomena are mainly caused by the following reasons: (1) μ -TiCN volume density (5.08 g/cm^3) is higher than that of Al_2O_3 . In the same unit volume, μ -TiCN content increases, μ - Al_2O_3 particles decrease and the overall density increases; (2) When the content of μ -TiCN exceeds the optimal value, the different van der Waals forces between particles lead to the aggregation of n - Al_2O_3 around the same type of μ - Al_2O_3 to form agglomeration, which produces pores of different sizes between these agglomeration and μ -TiCN (black hole in Figure 7f). Compared with Al_2O_3 with high hardness, μ -TiCN has lower internal stress and high toughness, which is also the key factor for the best performance of Al_2O_3 composite ceramic St2 with 10 wt % n - Al_2O_3 and 30 wt % μ -TiCN. This shows that the appropriate amount of n - Al_2O_3 and μ -TiCN is more conducive to the properties of Al_2O_3 composite ceramics.

4. Conclusions

In this study, Sn-x and St-x type Al_2O_3 composite ceramics were successfully prepared by the MEX-PPM process-based additive manufacturing with mixed micron-sized and nanosized particles as raw materials. The effects of n - Al_2O_3 and μ -TiCN on the mechanical properties and microstructure of Al_2O_3 composite ceramics were studied by degreasing, sintering and performance test. The following conclusions were listed as follows:

- (1) n - Al_2O_3 has a significant effect on the hardness of Al_2O_3 composite ceramics. The change in hardness of Sn-x type ceramics effected with n - Al_2O_3 was 1.118 GPa, which was higher than the change in St-x type ceramics effected with μ -TiCN (0.739 GPa). The volume density and porosity of 10 wt % n - Al_2O_3 ceramics are improved, which is better than that of the other Sn-x ceramics.
- (2) The volume density, flexural strength and fracture toughness of Al_2O_3 composite ceramics affected by μ -TiCN change significantly. The changes of volume density, flexural strength and fracture toughness of St-x type ceramics affected by optimum ratio 30 wt % μ -TiCN were at 0.257 g/cm^3 , 70.875 MP and 0.531 MPa/mm^2 , respectively, which were higher than the changes in Sn-x type ceramics effected with 10 wt % n - Al_2O_3 (0.091 g/cm^3 , 24 MPa and 0.205 MPa/mm^2).
- (3) The best ratio of 10 wt % n - Al_2O_3 and 30 wt % μ -TiCN optimized the microstructure and mechanical properties of Al_2O_3 composite ceramics. The porosity and volume density were at 4.073% and 4.177 g/cm^3 , and the hardness, flexural strength and fracture toughness were 16.592 GPa, 592.875 MPa and 6.308 MPa/mm^2 . The flexural strength of composite ceramics fabricated is higher than that of Al_2O_3 ceramics prepared by SLA in reference [27] ($178.84 \pm 17.66 \text{ MPa}$), which has the potential of high-pressure resistant structural materials.

Author Contributions: Conceptualization, X.H. and J.X.; methodology, X.H. and W.J.; formal analysis, X.H., J.X. and W.J.; writing—original draft preparation, X.H.; writing—review and editing, X.H., J.X. and W.J.; supervision, J.X. and W.J. All authors have read and agreed to the published version of the manuscript.

Funding: This research was funded by the National Natural Science Foundation of China (Grant No. 51805212), Natural Science Found of Jiangsu Province (Grant No. BK20160182) and the Major Scientific and the Technological Innovation Project of Shandong Province (Grant No. 2019JZZY020111).

Institutional Review Board Statement: Not applicable.

Informed Consent Statement: Not applicable.

Data Availability Statement: Data are available upon request from the corresponding author.

Conflicts of Interest: The authors declare no conflict of interest.

References

1. Jianxin, D.; Zhenxing, D.; Dongling, Y.; Hui, Z.; Xing, A.; Jun, Z. Fabrication and performance of Al₂O₃/(W,Ti)C+ Al₂O₃/TiC multilayered ceramic cutting tools. *Mater. Sci. Eng. A-Struct.* **2010**, *527*, 1039–1047. [[CrossRef](#)]
2. Norfauzi, T.; Hadzley, A.B.; Azlan, U.A.A.; Afuza, A.A.; Faiz, M.M.; Naim, M.F. Fabrication and machining performance of ceramic cutting tool based on the Al₂O₃-ZrO₂-Cr₂O₃ compositions. *Mater. Res. Technol.* **2019**, *8*, 5114–5123. [[CrossRef](#)]
3. Qu, X.; Wang, F.; Shi, C.; Zhao, N.; Liu, E.; He, C.; He, F. In situ synthesis of a gamma-Al₂O₃ whisker reinforced aluminium matrix composite by cold pressing and sintering. *Mater. Sci. Eng. A-Struct.* **2018**, *709*, 223–231. [[CrossRef](#)]
4. Du, J.; Tang, B.; Liu, W.; Zhang, T.; Peng, J.; Chen, H.; Lei, Y. Effects of annealing and firing in wet hydrogen on the dielectric breakdown strengths of alumina ceramics. *J. Adv. Ceram.* **2020**, *9*, 173–182. [[CrossRef](#)]
5. Ponder, R.I.; Safaei, M.; Anton, S.R. Fabrication and selection of surrogate knee implant bearings for experimental evaluation of embedded in-vivo sensors. *J. Mech. Behav. Biomed. Mater.* **2019**, *91*, 237–246. [[CrossRef](#)]
6. Ivanov, K.V.; Fortuna, S.V.; Kalashnikova, T.A.; Glazkova, E.A. Effect of Alumina Nanoparticles on the Microstructure, Texture, and Mechanical Properties of Ultrafine-Grained Aluminum Processed by Accumulative Roll Bonding. *Adv. Eng. Mater.* **2019**, *21*, 1701135. [[CrossRef](#)]
7. Han, D.; Yang, C.; Fang, N.X.; Lee, H. Rapid multi-material 3D printing with projection micro-stereolithography using dynamic fluidic control. *Addit. Manuf.* **2019**, *27*, 606–615. [[CrossRef](#)]
8. Zocca, A.; Colombo, P.; Gomes, C.M.; Günster, J.; Green, D.J. Additive Manufacturing of Ceramics: Issues, Potentialities, and Opportunities. *J. Am. Ceram. Soc.* **2015**, *98*, 1983–2001. [[CrossRef](#)]
9. Lakhdar, Y.; Tuck, C.; Binner, J.; Terry, A.; Goodridge, R. Additive manufacturing of advanced ceramic materials. *Prog. Mater. Sci.* **2021**, *116*, 100736. [[CrossRef](#)]
10. Chen, Z.; Li, Z.; Li, J.; Liu, C.; Lao, C.; Fu, Y.; Liu, C.; Li, Y.; Wang, P.; He, Y. 3D printing of ceramics: A review. *J. Eur. Ceram. Soc.* **2019**, *39*, 661–687. [[CrossRef](#)]
11. Hwa, L.C.; Rajoo, S.; Noor, A.M.; Ahmad, N.; Uday, M.B. Recent advances in 3D printing of porous ceramics: A review. *Curr. Opin. Solid State Mater. Sci.* **2017**, *21*, 323–347. [[CrossRef](#)]
12. Mao, M.; He, J.; Li, X.; Zhang, B.; Lei, Q.; Liu, Y.; Li, D. The Emerging Frontiers and Applications of High-Resolution 3D Printing. *Micromachines* **2017**, *8*, 113. [[CrossRef](#)]
13. Xing, H.Y.; Zou, B.; Lai, Q.G.; Huang, C.Z.; Chen, Q.H.; Fu, X.S.; Shi, Z.Y. Preparation and characterization of UV curable Al₂O₃ suspensions applying for stereolithography 3D printing ceramic microcomponent. *Powder Technol.* **2018**, *338*, 153–161. [[CrossRef](#)]
14. He, R.; Liu, W.; Wu, Z.; An, D.; Huang, M.; Wu, H.; Jiang, Q.; Ji, X.; Wu, S.; Xie, Z. Fabrication of complex-shaped zirconia ceramic parts via a DLP-stereolithography-based 3D printing method. *Ceram. Int.* **2018**, *44*, 3412–3416. [[CrossRef](#)]
15. Ghazanfari, A.; Li, W.; Leu, M.C.; Hilmas, G.E. A novel freeform extrusion fabrication process for producing solid ceramic components with uniform layered radiation drying. *Addit. Manuf.* **2017**, *15*, 102–112. [[CrossRef](#)]
16. Zhou, M.P.; Liu, W.; Wu, H.D.; Song, X.; Chen, Y.; Cheng, L.X.; He, F.P.; Chen, S.X.; Wu, S.H. Preparation of a defect-free alumina cutting tool via additive manufacturing based on stereolithography—Optimization of the drying and debinding processes. *Ceram. Int.* **2016**, *42*, 11598–11602. [[CrossRef](#)]
17. Schmidt, J.; Altun, A.A.; Schwentenwein, M.; Colombo, P. Complex mullite structures fabricated via digital light processing of a preceramic polysiloxane with active alumina fillers. *J. Eur. Ceram. Soc.* **2019**, *39*, 1336–1343. [[CrossRef](#)]
18. Chen, J.; Bao, E.; Huang, D.; Ding, Y.; Qiu, X. Extrusion Freeforming-Based 3D Printing of Ceramic Materials. *Mater. Trans.* **2020**, *61*, 2236–2240. [[CrossRef](#)]
19. Ghazanfari, A.; Li, W.; Leu, M.; Watts, J.; Hilmas, G. Mechanical characterization of parts produced by ceramic on-demand extrusion process. *Int. J. Appl. Ceram. Technol.* **2017**, *14*, 486–494. [[CrossRef](#)]
20. Pierin, G.; Grotta, C.; Colombo, P.; Mattevi, C. Direct Ink Writing of micrometric SiOC ceramic structures using a preceramic polymer. *J. Eur. Ceram. Soc.* **2016**, *36*, 1589–1594. [[CrossRef](#)]
21. Liu, W.; Li, M.; Nie, J.; Wang, C.; Li, W.; Xing, Z. Synergy of solid loading and printability of ceramic paste for optimized properties of alumina via stereolithography-based 3D printing. *Mater. Res. Technol.* **2020**, *9*, 11476–11483. [[CrossRef](#)]
22. Moghadasi, M.; Du, W.; Li, M.; Pei, Z.; Ma, C. Ceramic binder jetting additive manufacturing: Effects of particle size on feedstock powder and final part properties. *Ceram. Int.* **2020**, *46*, 16966–16972. [[CrossRef](#)]
23. Li, X.; Liu, C.; Sun, B.; Liu, X.; Zuo, Z.; Shu, Y.; Zeng, X.; Yi, J.; Chen, H.; Liu, Y.; et al. Refined grain size of ITO ceramic targets prepared by pressure slip casting and two-step sintering. *J. Eur. Ceram. Soc.* **2021**, *41*, 3501–3511. [[CrossRef](#)]
24. Liu, W.; Wu, H.; Zhou, M.; He, R.; Jiang, Q.; Wu, Z.; Cheng, Y.; Song, X.; Chen, Y.; Wu, S. Fabrication of fine-grained alumina ceramics by a novel process integrating stereolithography and liquid precursor infiltration processing. *Ceram. Int.* **2016**, *42*, 17736–17741. [[CrossRef](#)]
25. Xu-Guo, H.; Zi-Shang, C.; Xiao-Ping, L.; Sheng, B. Effect of sintering additives size on the microstructure and wear properties of Al₂O₃ ceramics. *Ferroelectrics* **2017**, *521*, 101–107. [[CrossRef](#)]
26. Wu, H.; Cheng, Y.; Liu, W.; He, R.; Zhou, M.; Wu, S.; Song, X.; Chen, Y. Effect of the particle size and the debinding process on the density of alumina ceramics fabricated by 3D printing based on stereolithography. *Ceram. Int.* **2016**, *42*, 17290–17294. [[CrossRef](#)]
27. Zhang, K.; He, R.; Ding, G.; Bai, X.; Fang, D. Effects of fine grains and sintering additives on stereolithography additive manufactured Al₂O₃ ceramic. *Ceram. Int.* **2021**, *47*, 2303–2310. [[CrossRef](#)]

28. Sun, C.; Tian, X.; Wang, L.; Liu, Y.; Wirth, C.M.; Günster, J.; Li, D.; Jin, Z. Effect of particle size gradation on the performance of glass-ceramic 3D printing process. *Ceram. Int.* **2017**, *43*, 578–584. [[CrossRef](#)]
29. He, X.; Xu, J.; Ji, W. The effect of surfactants on the performances of ceramic slurry by material extrusion and photo-polymerization combined molding process. *J. Ceram. Soc. Jpn.* **2021**, *129*, 489–495. [[CrossRef](#)]
30. Lóh, N.J.; Simão, L.; Justi, J.; Arcaro, S.; Raupp-Pereira, F.; De Noni, A.; Montedo, O.R.K. Densified alumina obtained by two-step sintering: Impact of the microstructure on mechanical properties. *Ceram. Int.* **2020**, *46*, 12740–12743. [[CrossRef](#)]